Structure and Dynamics of *N*-Isopropylacrylamide/Acrylic Acid Copolymer Gels Prepared by Cross-Linker-Free UV−Induced Polymerization

Takuya Suzuki,[†] Fumiyoshi Ikkai,[‡] and Mitsuhiro Shibayama*[,†]

Institute for Solid State Physics, The University of Tokyo, 5-1-5 Kashiwanoha, Kashiwa, Chiba 277-8581, Japan, and Nihon L'Oreal K.K., KSP R&D-D637, 3-2-1 Sakado, Takatsu-ku, Kawasaki, Kanagawa 213-0012, Japan

Received October 24, 2006; Revised Manuscript Received February 9, 2007

ABSTRACT: The structure and dynamics of poly(*N*-isopropylacrylamide-*co*-acrylic acid) (NIPAm/AAc) gels prepared either by cross-linker-free UV-induced polymerization or by redox polymerization were compared using swelling measurement and dynamic/static light scattering. Either AAc monomer or AAc polymer units are included in the polymer network. As a result, four types of NIPAm/AAc gels were obtained, namely (**A**) redox-mono, (**B**) UV-mono, (**C**) redox-poly, and (**D**) UV-poly. **A** is the reference polymer mostly investigated in the literature. The following facts emerged: Compared to **A**, **B** contains a large portion of defects, e.g., dangling chains, loops and branched chains, which leads to characteristic behavior, i.e., (i) larger swelling ratio and (ii) stronger temperature dependence of the spatial inhomogeneities. Charged groups in both **C** and **D** are topologically localized on AAc polymer chains, which result in different temperature dependencies of the structure and dynamics.

1. Introduction

Ionization is one of the most important factors, which affects phase separation and the microstructure of polymer gels. In the case of thermosensitive gels, such as poly(*N*-isopropylacrylamide)(NIPAm) gels,[1,2] a continuous volume-phase transition (VPT) takes place at around 33.8 °C. Charges, such as carboxy groups, can easily be introduced by copolymerizing NIPAm with acrylic acid (AAc). It results in dramatic changes in the phase behavior of gels. For example, VPT becomes discontinuous and the transition temperature shifts upward.[3] The discrete transition observed in NIPAm/AAc gels is explained by conventional thermodynamic theories on gel swelling, in which the Donnan potential is balanced against the free energy originating from entropy elasticity of polymer chains and mixing free energy.[4,5]

The microscopic events of VPT, on the other hand, have been extensively studied using various methods, including dynamic light scattering (DLS),[6] nuclear magnetic resonance (NMR),[7] and small-angle neutron scattering (SANS).[8,9] Shibayama et al. reported that a microphase separation took place during heating prior to a macroscopic discrete VPT.[2] Theoretical predictions of microphase separation for weakly charged polymer solutions in a poor solvent were proposed by Borue and Erukhimovich[10] and by others.[11] Then, they were altered to account for weakly charged polymer gels by Rabin and Panyukov.[12] SANS studies were also performed to investigate pH and salt concentration dependence of the microscopic structures of NIPAm/AAc gels.[5]

The characteristic repeat distance of microphase separated structure is estimated to be of the order of hundreds angstroms. The microphase separation has been interpreted as a sign that a swollen phase (ionized hydrophilic parts, AAc rich domains) and a shrunken phase (hydrophobic parts, NIPAm rich domains) coexist microscopically in NIPAm/AAc gels. Many theoretical works predict that the repeat distance of microphase separation depends on the degree of ionization in a gel.[12−15] Tanaka suggested that a VPT was caused by competition of molecular interactions, i.e., hydrogen bonding, electrostatic repulsion, and hydrophobic interactions and that it was strongly related to life activities in biological body.[16,17] Indeed, Annaka and Tanaka discovered multiple VPT, in which a gel could have several stable phases depending on environmental conditions.[16] They concluded that this behavior resulted from nonrandom configuration of co-monomer units with competing interactions, indicating that local segment order could play a prominent role in determining the gel microstructure. It has been assumed that ionized groups, e.g., carboxy groups, were randomly distributed on the polymer network as monomer units. Otherwise, the degree of ionization cannot be taken as an average of overall gel (mean-field approximation). If charge-carrying monomers are nonrandomly distributed on network chains, what happens to microscopic gel structures? In this study, we investigated how spatial configurations of weakly charged groups in a gel network affected its microstructure and dynamics.

2. Theoretical Background

As is known, the intensity−time correlation function (ICF) for a gel at a sample position p, $g_p^{(2)}(q,\tau) - 1$, is approximated to be a single-exponential function as far as it is far from its critical point,[18]

$$g_p^{(2)}(q,\tau) - 1 = \beta\sigma_{I,p}{}^2 \exp[-2D_{A,p}q^2\tau] \qquad (1)$$

where β is the instrumental coherence factor (≈ 0.95 in this study) and q is the magnitude of the scattering vector. Note that gels are nonergodic media, and hence ICF is dependent on the sample position.[19−21] $\sigma_{I,p}{}^2$ is the initial amplitude of the correlation function and $D_{A,p}$ is the apparent diffusion coefficient at p. On the other hand, when the gel is near the critical point or has large structural inhomogeneities, the ICF becomes a complex function. However, even in this case, because the gel still has a single-exponential component at the small τ region, $D_{A,p}$ can be estimated by the initial slope of $g_p^{(2)}(q,\tau) - 1$, i.e.,

* To whom correspondence should be addressed. E-mail: shibayama@issp.u-tokyo.ac.jp.
[†] Institute for Solid State Physics, The University of Tokyo.
[‡] Nihon L'Oreal K.K.

10.1021/ma062448b CCC: $37.00
Published on Web 03/13/2007

$$D_{A,p} = -\left(\frac{1}{2q^2}\right)\lim_{\tau\to 0}\frac{\partial \ln[g_p^{(2)}(q,\tau)-1]}{\partial \tau} \quad (2)$$

According to Joosten et al.,[22] the collective diffusion coefficient of a nonergodic medium, D, can be evaluated by plotting $D_{A,p}$ as a function of the time average scattered intensity at p, $\langle I\rangle_{T,p}$, using the following relationship

$$D_{A,p} = \frac{D}{2-\langle I_F\rangle_T/\langle I\rangle_{T,p}} \quad (3)$$

where $\langle I_F\rangle_T$ is the fluctuating part of $\langle I\rangle_{T,p}$. Note that $\langle I_F\rangle_T$ is independent of p. Equation 3 can be rewritten as follows:

$$\frac{\langle I\rangle_{T,p}}{D_{A,p}} = \frac{2}{D}\langle I\rangle_{T,p} - \frac{\langle I_F\rangle_T}{D} \quad (4)$$

This means that we can evaluate $\langle I_F\rangle_T$ and D by a linear regression of a $\langle I\rangle_{T,p}/D_{A,p}$ vs $\langle I\rangle_{T,p}$ plot.[23] Once $\langle I_F\rangle_T$ is evaluated, the static inhomogeneities can be easily extracted from

$$\langle I_C\rangle_E \equiv \langle I\rangle_E - \langle I_F\rangle_T \quad (5)$$

where $\langle I_C\rangle_E$ denotes the time-independent term of the ensemble average scattered intensities, $\langle I\rangle_E$, i.e., a measure of the degree of spatial inhomogeneities. Thus, we can split up the observed scattering intensity, $\langle I\rangle_E$, into the frozen inhomogeneities, $\langle I_C\rangle_E$, and the fluctuating component, $\langle I_F\rangle_T$. In order to discuss the dynamics of gels, it is more convenient to use the ensemble-averaged ICF rather than the time averaged ICF defined in eq 1

$$\langle g^{(2)}(q,\tau)\rangle_E \equiv \frac{\frac{1}{N}\sum_p^N \langle I(q)\rangle^2_{T,p} g_p^{(2)}(q,\tau)}{\left\{\frac{1}{N}\sum_p^N \langle I(q)\rangle_{T,p}\right\}^2} \quad (6)$$

where $I(q)$ is the scattering intensity at the magnitude of scattering vector q and N is the number of sampling points.[19,24,25]

3. Experimental Section

3.1. Samples. We prepared four types of NIPAm/AAc copolymer gels using two polymerization methods. Figure 1 shows a diagram of those copolymer gels. The lattice-shaped boxes represent gel networks, where each of fine and thick lines on grids corresponds to NIPAm and AAc monomer units, respectively. The small closed circles denote cross-linkages. Parts A and B of Figure 1 show NIPAm/AAc copolymer gels in which NIPAm and AAc are randomly copolymerized as monomer units by conventional redox polymerization (code: redox-mono) and by UV-induced polymerization (code: UV-mono), respectively.[26,27] On the other hand, parts C and D of Figure 1 show NIPAm/AAc gels in which AAc polymer chains are either physically entrapped (code: redox-poly) or chemically linked to NIPAm network (code: UV-poly). It should be noted that these four types of gels have the same degree of ionization stoichiometrically, i.e., the same ratio of AAc monomer units to NIPAm units, but different spatial configurations of weakly charged groups.

3.2. Gel Preparation (A, Redox-Mono). A 6.68 mmol sample of NIPAm monomer (Kohjin Chemical Co. Ltd.) and 0.32 mmol of acrylic acid (AAc) (Wako Chemical Co.) were dissolved in 10 mL of deionized water. Then, 0.07 mmol of *N*,*N*′-methylenebis-(acrylamide) (BIS) and 0.0154 mmol of ammonium persulfate (APS) were added to the solution as cross-linker and redox-initiator, respectively. After further addition of 24 μL of *N*,*N*,*N*′,*N*′-tetramethylethylenediamine (TEMED) as accelerator, the solution was kept at 20 °C for 24 h for gelation.

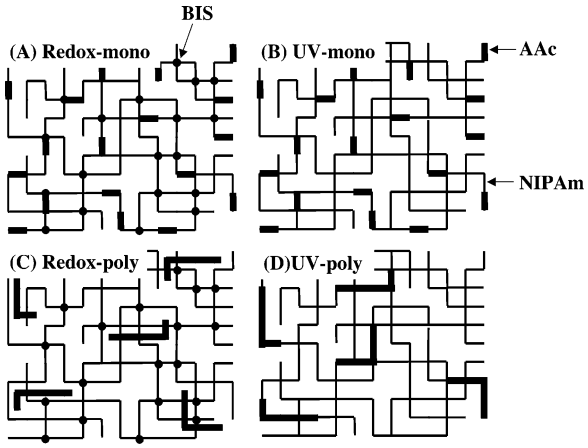

Figure 1. Schematic representation of the four types of NIPAm/AAc gels: (**A**) redox-mono, (**B**) UV-mono, (**C**) redox-poly, and (**D**) UV-poly. Thin and thick lines denote NIPAm and AAc segments, respectively. BIS cross-linkers are represented by small closed circles. Note that AAc polymer chains in (**C**) redox-poly are physically entrapped in NIPAm network, while those in (**D**) UV-poly are chemically bonded to NIPAm network.

(B, UV-Mono). An aqueous solution containing 668 mM NIPAm, 32 mM AAc, and 20 mM APS (as UV-photoinitiator) was exposed to UV radiation provided by a 500 W Deep-UV lamp (USHIO Inc., Tokyo, Japan) with an illuminance spectrum including a range of wavelengths lower than 300 nm.[26] UV irradiation was carried out by using a parallel light irradiated from the side of the test tube. The area of irradiation was large enough to cover the sample.[28] The optical density of the pregel solution was about 0.7 at 254 nm. Gel was produced following UV-irradiation for 1 h at 20 °C.

(C, Redox-Poly). A 6.68 mmol sample of NIPAm, 0.32 mmol (expressed as monomer units) of AAc polymer (M_w = 118 000 and M_w/M_n = 1.13, M_w and M_n being the weight- and number-average molecular weights, respectively), 0.07 mmol of BIS, 0.0154 mmol of APS, and 24 μL of TEMED were dissolved in 10 mL of deionized water and then kept at 20 °C for 24 h for gelation.

(D, UV-Poly). Aqueous solution containing 668 mM NIPAm, 32 mM (expressed as monomer units) AAc polymer, and 20 mM APS (as UV-photoinitiator) was exposed to UV-irradiation for 1 h at 20 °C to produce a gel.

The polymerizations of all gel samples were carried out at pH 8 where acrylic acid was ionized. Cross-linking of AAc polymers by UV-irradiation has been confirmed elsewhere.[26] Certainly, it is highly expected that some degradation would occur by UV irradiation as well. For DLS measurements, the thereby prepared samples were used as such without further treatment. For swelling measurements, each of gel samples was prepared in a narrow quartz capillary (ca. 800 μm diameter) and washed with an excess amount of water. In addition, NIPAm homopolymer gels were also prepared using either redox- or UV-polymerization method for studying the effect of UV-polymerization compared to redox one on the swelling properties, microstructures, and dynamics.

3.3. Swelling Degree Measurements. The sample was immersed in a thermostated chamber filled with distilled water. The degree of swelling, d/d_0, was measured by monitoring the diameter of the cylindrical gel, d, via an inverted microscope (TMD300, Nikon, Co., Ltd, Tokyo, Japan) coupled with an image processor (Algas 2000, Hamamatsu Photonics, Co., Ltd, Hamamatsu, Japan). d_0 is the gel diameter at preparation time. Whenever the temperature was changed, the maximum width of the gel was measured with an interval of 20 min to a few hours until two successive widths became identical. The measurement was repeated at least three times and the average was used as the d value.

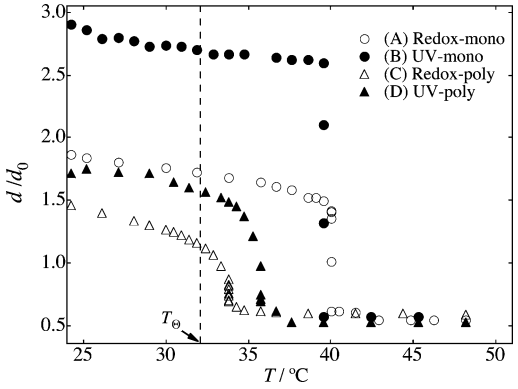

Figure 2. Temperature variations of the equilibrium linear swelling ratio, d/d_0, for the NIPAm/AAc gels. Here, d and d_0 are the diameters of gels at observation and at preparation time, respectively. The dashed line indicates T_Θ, the so-called Θ-temperature for NIPAm aqueous solutions.

3.4. DLS Measurements. DLS studies were carried out using a DLS/SLS-5000 compact goniometer, ALV, Langen, coupled with an ALV photon correlator. A 22 mW helium−neon laser (wavelength, $\lambda = 6328$ Å) was used to deliver the incident beam. The decay rate distribution functions $G(\Gamma)$ were calculated from ICF using the CONTIN data analysis package. All the DLS measurements were conducted for as-prepared gels. Hence the polymer concentration was 700 mM (i.e., $d/d_0 = 1.00$). The scattering angle was 90° ($q \approx 0.00187$ Å^{-1} in aqueous media) except for q-dependent measurements.

4. Results and Discussion

4.1. Swelling Degree Measurements. Figure 2 shows the temperature dependence of the swelling degree of all gel samples on heating. As is well-known, NIPAm hydrogels undergo a shrinking transition at a VPT temperature, $T_{VPT} \approx 34$ °C.[1] This temperature is slightly higher than the so-called Θ-temperature of NIPAm polymer aqueous solutions ($T_\Theta \approx 32$ °C).[29] The difference between T_{VPT} and T_Θ is ascribed to the presence of elastic free energy in gels in addition to the enthalpy and entropy of mixing whereas the phase behavior of polymer solutions are determined by the last two terms.[30,31] Introducing charged AAc groups into NIPAm polymer gels results in a significant shift of T_{VPT} and swelling ratio at equilibrium.[3] As a matter of fact, in the case of (**A**) redox-mono, the transition is discontinuous and T_{VPT} (≈ 40 °C) is much higher than T_Θ. For (**B**) UV-mono, T_{VPT} is almost the same as **A**. Note that the swelling degree of **B** at the swollen state is much higher than that of **A**. This indicates that effective cross-linking density (CD) of **B** is much lower than **A**. (**C**) Redox-poly, on the other hand, shrunk at ca. 34 °C, showing a similar behavior as NIPAm homopolymer gel. This suggests that AAc polymers in **C** do not play any role at all because of physical entrapment into NIPAm network. (**D**) UV-poly exhibited an intermediate behavior. It shrunk at a temperature between 34 °C and 40 °C and the degree of swelling at lower temperatures ($< T_{VPT}$) was also between the two extremes. This was a clear evidence of chemical cross-linking of AAc polymer chains to NIPAm network. It also indicated that the cross-linking affected both the T_{VPT} and swelling behavior.

4.2. Visual Observation of Turbidity. A series of photographs of the gels taken at different temperatures are shown in Figure 3. In the case of (**A**) redox-mono, the gel was transparent even at 35.0 °C. This is normal since the gel has not reached its T_{VPT} (≈ 40 °C) yet. On the other hand, (**B**) UV-mono started to become opaque at T_Θ and completely became opaque at 35.0 °C. Note that the opaque area emerged from the bottom. This

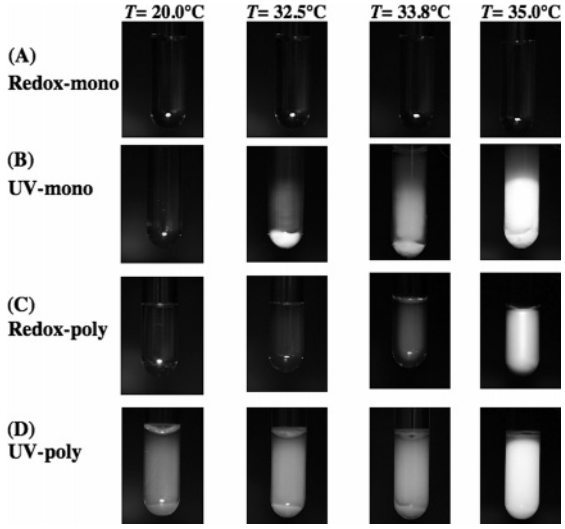

Figure 3. Series of photographs showing clarity/opacity of the four types of gels at different temperatures.

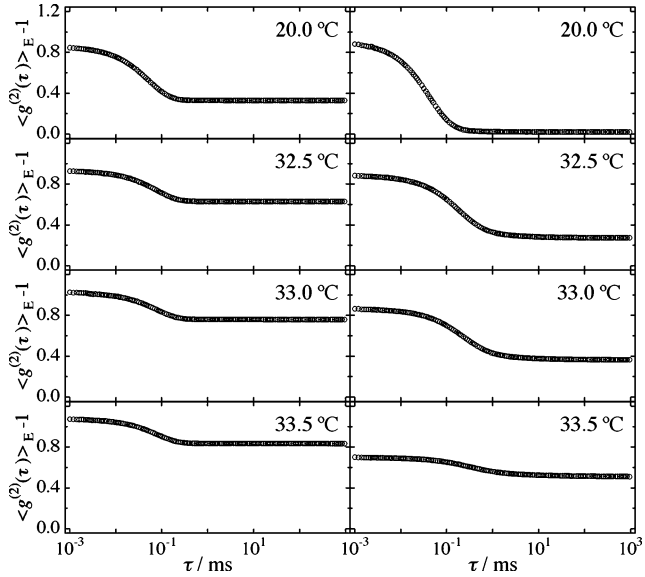

Figure 4. Time−intensity correlation functions (ICFs) for the homopolymer gels: (left) redox-NIPAm and (right) UV−NIPAm at various temperatures.

is mainly due to lack of UV irradiation at the bottom of the tube because of its round shape of the test tube. (**C**) Redox-poly turned opaque at 33.8 °C as did NIPAm homopolymer gels. (**D**) UV-poly, on the other hand, showed opacity from the beginning. This suggests that UV-induced NIPAm polymerization in the presence of AAc polymer chains leads to phase separation between NIPAm rich and AAc rich domains. It may be the reason why **D** shows intermediate properties between **B** and **C**.

4.3. Dynamic Light Scattering (DLS). 4.3.1. Homopolymer Gels. Before tackling the characteristic features and properties of the products from different gelation methods, let us first discuss the structure of NIPAm homopolymer gels prepared by redox- and UV-polymerization, coded respectively as redox-NIPAm and UV−NIPAm. Figure 4 shows ensemble-averaged ICFs, $\langle g^{(2)}(\tau)\rangle_E - 1$, of redox-NIPAm (left column) and UV−NIPAm (right column) at various temperatures. Here, 100 (=N in eq 6) sample positions were arbitrarily chosen and time-averaged ICFs were obtained with a nonergodic measurement option provided by ALV by employing eq 6. It should be noted here that $\langle g^{(2)}(\tau = 0)\rangle_E - 1$ is expected to be unity.[19] However,

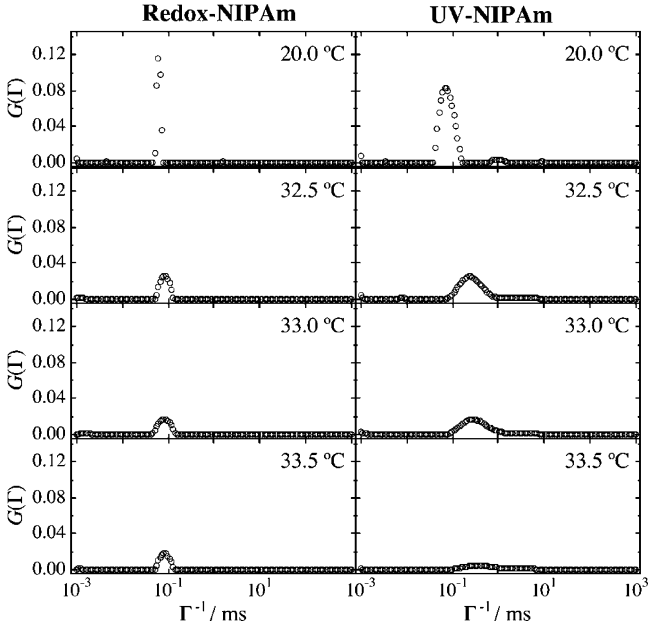

Figure 5. Distribution functions, $G(\Gamma)$s, for the homopolymer gels: (left) redox-NIPAm and (right) UV−NIPAm at various temperatures.

as shown in the figures, the values deviated from unity in most of the cases. This is mainly due to the following two reasons. (1) The number of sampling points $N = 100$ was not enough. (2) Due to very strong scattering from gels at high Ts, we had to reduce the incident beam intensity, resulting in significant counting-losses from weak scattering points in gels and a deviation from a Poisson distribution of scattering intensities. At 20 °C, i.e., at a temperature much lower than the macroscopic volume-phase transition temperature, T_{VPT}, both series show a single decay around $\tau \approx 10^{-1}$ ms. The plateau value of UV−NIPAm is much lower than that of redox-NIPAm. This means that UV−NIPAm has a larger contribution of the dynamic component than redox-NIPAm. This result is consistent with the result of the swelling measurements. When temperature was increased, redox-NIPAm kept a single decay behavior at temperatures lower than T_{VPT}, and the plateau value increased further. The same trend was observed in UV−NIPAm.

Figure 5 shows the corresponding distribution functions, $G(\Gamma)$, where Γ is the characteristic decay rate. The difference discussed in relation to Figure 4 is clearly seen in this figure. Although peak broadening is observed in both gels, the gel dynamics, represented by a single "gel-mode"[32] (or collective mode),[18] is rather preserved at $\Gamma^{-1} \approx 10^{-1}$ ms for redox-NIPAm even at the elevated temperature. On the other hand, UV−NIPAm shows a significant peak broadening accompanying a peak shift to a larger Γ^{-1}. This means a critical slowing down by approaching VPT.[33]

4.3.2. Copolymer Gels. Temperature dependence of scattering behavior of the four types of NIPAm/AAc copolymer gels is shown in Figure 6, in which $\langle I\rangle_E$, $\langle I_F\rangle_T$, and $\langle I_C\rangle_E$ are plotted vs T. As defined by eq 5, $\langle I\rangle_E$, $\langle I_F\rangle_T$, and $\langle I_C\rangle_E$ are the ensemble-averages of the speckle intensities, the position-independent fluctuating component, and the time-independent frozen component of $\langle I\rangle_{T,p}$, respectively. The scattering intensities of (**A**) redox-mono increase gradually with T. Here, no strong amplification was observed even going beyond its T_{VPT} (≈ 40 °C). On the other hand, (**B**) UV-mono shows a divergence at ca. 33 °C in spite of T_{VPT} around 40 °C. This comparison indicates that the structure of **B** is very different from that of **A**. In the case of **A**, spatial inhomogeneities are suppressed over a wide

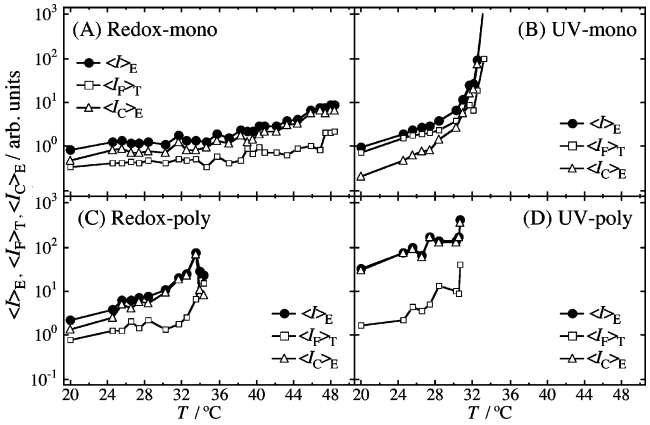

Figure 6. Temperature variations of $\langle I\rangle_E$, $\langle I_F\rangle_T$, and $\langle I_C\rangle_E$ for (**A**) redox-mono, (**B**) UV-mono, (**C**) redox-poly, and (**D**) UV-poly.

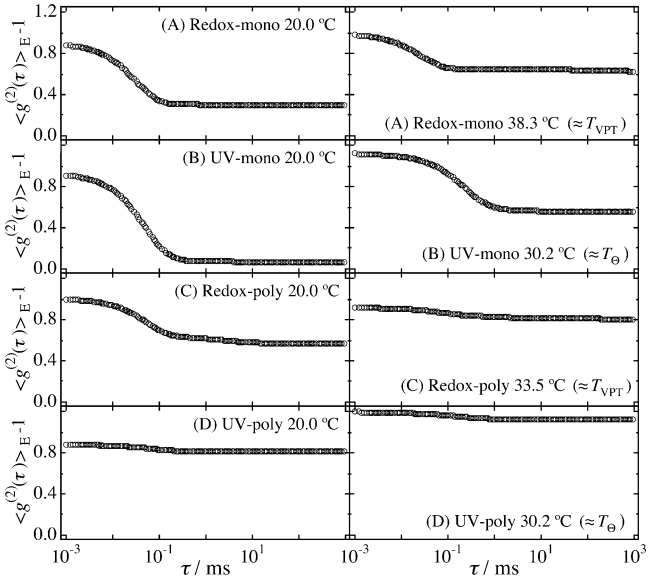

Figure 7. Time−intensity correlation functions (ICFs) for (**A**) redox-mono, (**B**) UV-mono, (**C**) redox-poly, and (**D**) UV-poly at 20 °C (far below T_{VPT}; left) and at high temperatures (right).

temperature range due to a high osmotic pressure originating from the Donnan potential created by charged AAc groups within the network.[4,5] It is also interesting to note that, for **B**, $\langle I_F\rangle_T$ is larger than $\langle I_C\rangle_E$ at low temperatures and they crossover at a temperature around T_Θ. However, the divergence observed in **B** clearly suggests that charges from ionized AAc do not play a significant role, and the gel behaves in a similar way as NIPAm homopolymer gels. (**C**) Redox-poly also shows a similar trend as **B**. $\langle I\rangle_E$ of (**D**) UV-poly seems to have strong frozen inhomogeneities inherently. This is why the temperature variations of $\langle I\rangle_E$, $\langle I_F\rangle_T$, and $\langle I_C\rangle_E$ are weaker compared to other systems. Note that $\langle I\rangle_E$ and $\langle I_C\rangle_E$ for **D** cannot be distinguished since $\langle I_F\rangle_T$ is much smaller than $\langle I\rangle_E$ and $\langle I_C\rangle_E$.

Figure 7 shows a series of ensemble-averaged ICFs, $\langle g^{(2)}(\tau)\rangle_E - 1$, at 20.0 °C (left; sample-prepared temperature) and at temperature near T_{VPT} or T_Θ (right). Here, T_Θ was exclusively chosen when a DLS measurement at T_{VPT} was not possible due to sample clouding. In the case of **A** and **B**, the ICF seems to have a characteristic decay corresponding to the gel mode with $\tau \approx 10^{-1}$ ms at 20.0 °C. At 38.3 °C for **A**, the gel mode remains. This temperature is close to T_{VPT}. On the other hand, for **B**, a characteristic decay time with $\tau \approx 10^{-1}$ ms at 20.0 °C shifts to a larger τ at 30.2 °C as a result of critical slowing down.[33,34] In the case of **C**, a drastic change in ICFs

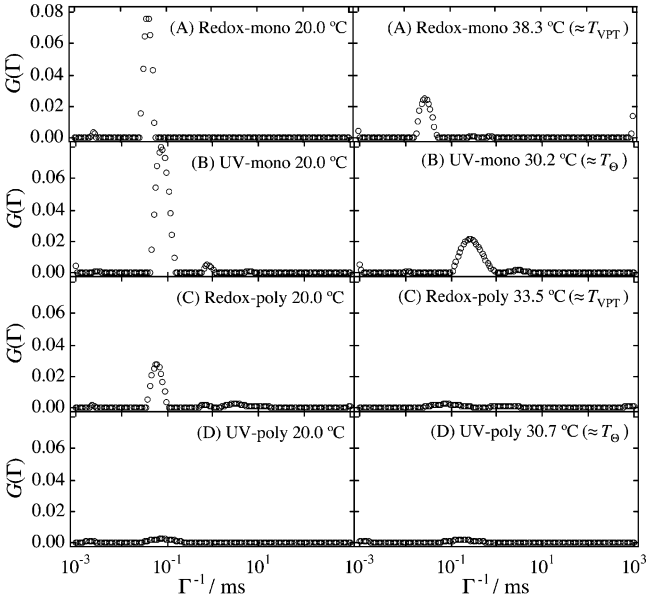

Figure 8. Distribution functions, $G(\Gamma)$s, for (**A**) redox-mono, (**B**) UV-mono, (**C**) redox-poly, and (**D**) UV-poly at 20 °C (far below T_{VPT}; left) and at high temperatures (right).

between the two temperatures is observed. At 20 °C, it holds the gel mode. On the other hand, frozen components are dominant at 33.5 °C (≈ T_{VPT}). **D** has large fronzen inhomogeneities even at 20 °C and the inhomogeneities become much larger by increasing temperature to 30.2 °C (≈T_Θ). Note that all of these characteristic properties are well correlated to the behavior of the scattering intensities as discussed in relation to Figure 6. Figure 8 shows the corresponding distribution functions, $G(\Gamma)$s. First of all, a peak shift of the gel mode is clearly seen for **A** at 20 °C toward the smaller Γ^{-1} region with respect to that of redox-NIPAm (Figure 5). This is due to the effect of charges distributed homogeneouly in the network. An increase in T resulted in a peak shift as well as broadening as discussed above. Similar behaviors are observed in **B**. Although **C** had the gel mode at 20 °C, it disappeared at 33.5 °C (≈ T_{VPT}). Interestingly, **D** does not have the gel mode both at 20 °C and T_Θ. This means that **D** is phase-separated irrespective of temperature as indicated in Figures 3 and 7, and has very little small dynamic components.

Figure 9 shows q dependence of the decay rate Γ for the mode mode. The upper column shows those at 20 °C and the lower at the high temperatures. As shown here, the gel mode clearly shows q^2 dependence of Γ, confirming that the collective motion is a diffusive mode as first discussed by Tanaka et al.[18]

4.4. Static Structures. Figure 10 shows static light scattering (LS) intensity functions, $I(q)$, as a function of q for (**A**) redox-mono, (**B**) UV-mono, (**C**) redox-poly, and (**D**) UV-poly at 20.0 °C and at a high temperature. The scattering intensity functions obtained with small-angle neutron scattering (SANS) were also plotted in order to compare the structure factors of the gels in a broad q range. Although the details of SANS experiments and the discussions are given elsewhere,[35] SANS results show marked difference in the samples prepared by different methods. It is rather surprising that no significant q dependence is observed for all of gels in the LS regime, but the magnitudes of $I(q)$s are quite different depending on the samples and are in good agreement with the results shown in Figure 6. The SANS results, on the other hand, show strong T dependence in $I(q)$.[35] In particular, except for redox-poly, a distinct peak appears in $I(q)$ at high temperatures, suggesting the existence of microphase separated structure. Hence, it is clear that the gel samples made

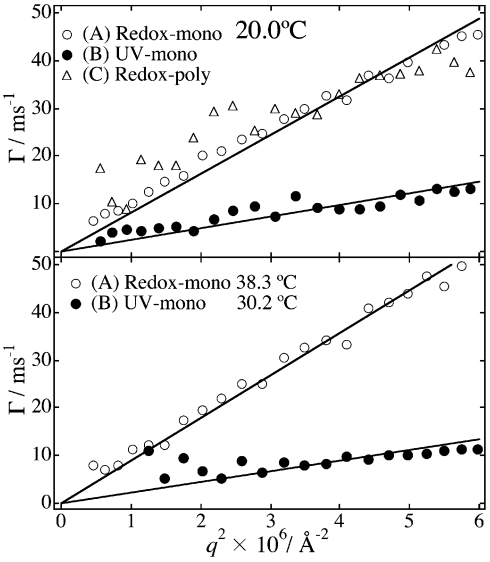

Figure 9. q dependence of the decay rate Γ for the gel mode of (**A**) redox-mono, (**B**) UV-mono, and (**C**) redox-poly.

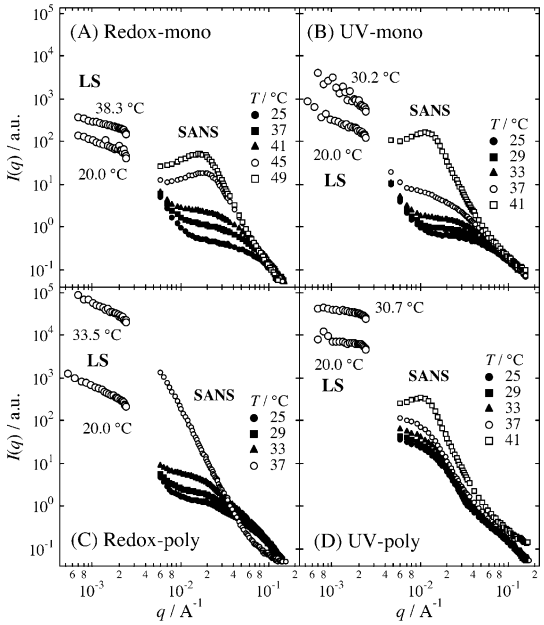

Figure 10. Static light scattering (LS) intensity and small-angle neutron scattering intensity functions, $I(q)$ for (**A**) redox-mono, (**B**) UV-mono, (**C**) redox-poly, and (**D**) UV-poly at 20.0 °C and at a high temperature.

with the four methods have different microscopic structures. Extensive discussions on SANS results are given elsewhere.[35]

4.5. Structure−Property Relationship. Figure 11 shows schemata of the NIPAm/AAc gels investigated in the present work. Here, the size of circles denotes the macroscopic swelling degree with respect to the volume of shrunken phases. The thick segments and lines indicate AAc monomer and AAc polymer chains, respectively. For (**A**) redox-mono, gel networks are relatively well-formed with a high efficiency of cross-linking. (**B**) UV-mono, on the other hand, has much fewer cross-linking points, and both topological and connection inhomogeneities, resulting in the production of a loose network. It is the reason why **B** swells larger than **A** at low temperatures. In the case of **A**, even though hydrophobic interactions of NIPAm networks become prominent when coming near to T_{VPT}, cross-linking points prevent NIPAm chains from moving. The gel keeps homogeneous structure as a result and collective diffusion mode still remains. Unlike **A**, **B** becomes an extremely inhomogeneous

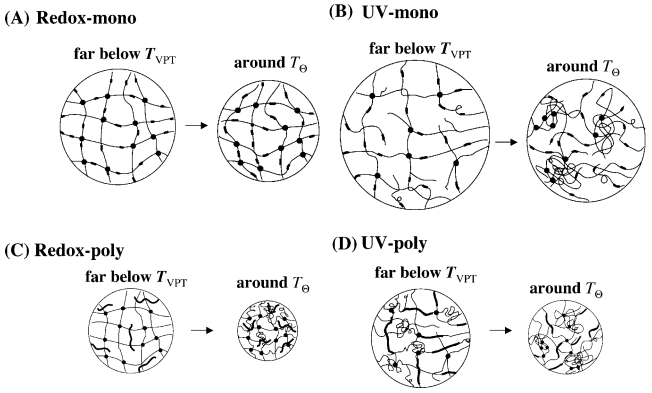

Figure 11. Diagram models showing the microscopic structures of (**A**) redox-mono, (**B**) UV-mono, (**C**) redox-poly, and (**D**) UV-poly. The circles represent the relative size of the gel, i.e., the degree of swelling. Thin lines, thick lines, and thick segments denote NIPAm chains, AAc polymer chains, and AAc segments, respectively. Dots indicate cross-linking points.

structure with increasing temperature. The lower cross-linking density as well as network defects lead to a more inhomogeneous structure in low cross-linked gels than in high cross-linked gels as previously reported by Ikkai et al. (the inversion phenomena in cross-link density dependence in gel inhomogeneities).[36,37] We infer that the characteristic loose network structure of **B** leads to a divergence of frozen inhomogeneities at ca. 33 °C based on DLS measurements despite T_{VPT} being ca. 40 °C.

In the case of (**C**) redox-poly, AAc polymer chains are not copolymerized but physically entrapped in the polymer network. Hence, the charge effects are not observed in swelling and DLS measurements. In the case of (**D**) UV-poly, AAc polymer chains are expanded due to the dissociation of the charged AAc polymer connected to NIPAm. As a result, the NIPAm network aggregates to some extent even far below T_{VPT}. This structure led to the extremely large static inhomogeneities even at low temperatures (e.g., 20 °C). Further structure investigation on these gels is underway.

5. Concluding Remarks

The structure and dynamics of four types of NIPAm/AAc gels, which were prepared using different reaction methods and have different spatial configurations of weakly charged AAc groups, were investigated by swelling measurements and dynamic light scattering (DLS). For (**A**) redox-mono, no inhomogeneities of gel network were seen over a wide range of temperatures and the volume-transition temperature, T_{VPT}, increased as has been reported so far. On the other hand, for (**B**) UV-mono, while the gel showed weak speckle pattern at low temperatures, the spatial inhomogeneities dramatically increased when coming near to the T_{VPT} of NIPAm, 34 °C ($\approx T_\Theta$) despite existing repulsive forces due to electrostatic interactions among ionized AAc groups. For (**C**) redox-poly, the swelling behavior and scattering properties were almost the same as in NIPAm homopolymer gels because of the physical entrapment of AAc polymer chains in the polymer network. For (**D**) UV-poly, the spatial inhomogeneities were extremely large even at temperatures far below T_{VPT} due to localized charged groups, i.e., carboxy groups chemically cross-linked to NIPAm.

Acknowledgment. This work was partially supported by the Ministry of Education, Science, Sports and Culture, Japan (Grant-in-Aid for Scientific Research (A), 2006-2008, No. 18205025, and for Scientific Research on Priority Areas, 2006-2010, No. 18068004)).

References and Notes

(1) Hirokawa, Y.; Tanaka, T. *J. Chem. Phys.* **1984**, *81*, 6379−6380.
(2) Shibayama, M.; Tanaka, T.; Han, C. C. *J. Chem. Phys.* **1992**, *97*, 6842−6854.
(3) Hirotsu, S.; Hirokawa, Y.; Tanaka, T. *J. Chem. Phys.* **1987**, *87*, 1392−1395.
(4) Ricka, J.; Tanaka, T. *Macromolecules* **1984**, *17*, 2916−2921.
(5) Shibayama, M.; Ikkai, F.; Inamoto, S.; Nomura, S.; Han, C. C. *J. Chem. Phys.* **1996**, *105*, 4358−4366.
(6) Tanaka, T.; Ishiwata, S.; Ishimoto, C. *Phys. Rev. Lett.* **1977**, *38*, 771−774.
(7) Tokuhiro, T.; Amiya, T.; Mamada, A.; Tanaka, T. *Macromolecules* **1991**, *24*, 2936−2943.
(8) Shibayama, M.; Tanaka, T.; Han, C. C. *J. Chem. Phys.* **1992**, *97*, 6829−6841.
(9) Shibayama, M.; Tanaka, T. *J. Chem. Phys.* **1995**, *102*, 9392−9400.
(10) Borue, V.; Erukhimovich, I. *Macromolecules* **1988**, *21*, 3240−3249.
(11) Joanny, J. F.; Leibler, L. *J. Phys. (Paris)* **1990**, *51*, 545−557.
(12) Rabin, Y.; Panyukov, S. *Macromolecules* **1997**, *30*, 301−312.
(13) Onuki, A. *Adv. Polym. Sci.* **1993**, *109*, 63−121.
(14) Panyukov, S.; Rabin, Y. *Macromolecules* **1996**, *29*, 8530−8537.
(15) Sasaki, S.; Maeda, H. *Phys. Rev. E* **1996**, *54*, 2761−2765.
(16) Annaka, M.; Tanaka, T. *Nature* **1992**, *355*, 430−432.
(17) Tanaka, T.; Sun, S. T.; Hirokawa, Y.; Katayama, S.; Kucera, J.; Hirose, Y.; Amiya, T. *Nature* **1987**, *325*, 796.
(18) Tanaka, T.; Hocker, L. O.; Benedek, G. B. *J. Chem. Phys.* **1973**, *59*, 5151−5159.
(19) Pusey, P. N.; van Megen, W. *Physica A* **1989**, *157*, 705−741.
(20) Joosten, J. G. H.; Gelade, E. T. F.; Pusey, P. N. *Phys. Rev. A* **1990**, *42*, 2161−2175.
(21) Xue, J. Z.; Pine, D. J.; Milner, S. T.; Wu, X. L.; Chaikin, P. M. *Phys. Rev. A* **1992**, *46*, 6550−6563.
(22) Joosten, J. G. H.; McCarthy, J. L.; Pusey, P. N. *Macromolecules* **1991**, *24* (25), 6690−6699.
(23) Shibayama, M.; Takata, S.; Norisuye, T. *Physica A* **1998**, *249*, 245−252.
(24) Shibayama, M. *Macromol. Chem. Phys.* **1998**, *199*, 1−30.
(25) Shibayama, M.; Karino, T.; Okabe, S. *Polymer* **2006**, *47*, 6446−6456.
(26) Ikkai, F.; Adachi, E. *Macromol. Rapid Commun.* **2004**, *25*, 1514−1517.
(27) Ikkai, F.; Shibayama, M. *J. Polym. Sci., Part B: Polym. Phys. Ed.* **2005**, *43*, 617−628.
(28) Ikkai, F.; Adachi, E. *Macromol. Chem. Phys.* **2007**, *208*, 271−276.
(29) Schild, H. G. *Prog. Polym. Sci.* **1992**, *17*, 163−249.
(30) Tanaka, T. *Phys. Rev. Lett.* **1978**, *40*, 820−823.
(31) Shibayama, M.; Tanaka, T. *Adv. Polym. Sci.* **1993**, *109*, 1−62.
(32) Norisuye, T.; Takeda, M.; Shibayama, M. *Macromolecules* **1998**, *31*, 5316−5322.
(33) Tanaka, T.; Sato, E.; Hirokawa, Y.; Hirotsu, S.; Peetermans, J. *Phys. Rev. Lett.* **1985**, *55*, 2455−2458.
(34) de Gennes, P. G. *Scaling Concepts in Polymer Physics*; Cornell University: Ithaca, NY, 1979.
(35) Ikkai, F.; Suzuki, T.; Karino, T.; Shibayama, M. *Macromolecules* **2007**, *40*, 1140−1146.
(36) Ikkai, F.; Shibayama, M. *Phys. Rev. E* **1997**, *56*, R51−R54.
(37) Shibayama, M.; Ikkai, F.; Shiwa, Y.; Rabin, Y. *J. Chem. Phys.* **1997**, *107*, 5227−5235.

MA062448B